



HAL
open science

What do stirred yogurt microgels look like? Comparison of laser diffraction, 2D dynamic image analysis and 3D reconstruction

Marine Moussier, Valérie Guenard-Lampron, Kevin Lachin, Gabrielle Moulin, Sylvie L. Turgeon, Camille Michon, Delphine Huc-Mathis, Véronique Bosc

► To cite this version:

Marine Moussier, Valérie Guenard-Lampron, Kevin Lachin, Gabrielle Moulin, Sylvie L. Turgeon, et al.. What do stirred yogurt microgels look like? Comparison of laser diffraction, 2D dynamic image analysis and 3D reconstruction. *Food Structure*, 2019, 20, 10.1016/j.foostr.2019.100107 . hal-02620143

HAL Id: hal-02620143

<https://hal.inrae.fr/hal-02620143>

Submitted on 22 Oct 2021

HAL is a multi-disciplinary open access archive for the deposit and dissemination of scientific research documents, whether they are published or not. The documents may come from teaching and research institutions in France or abroad, or from public or private research centers.

L'archive ouverte pluridisciplinaire **HAL**, est destinée au dépôt et à la diffusion de documents scientifiques de niveau recherche, publiés ou non, émanant des établissements d'enseignement et de recherche français ou étrangers, des laboratoires publics ou privés.



Distributed under a Creative Commons Attribution - NonCommercial 4.0 International License

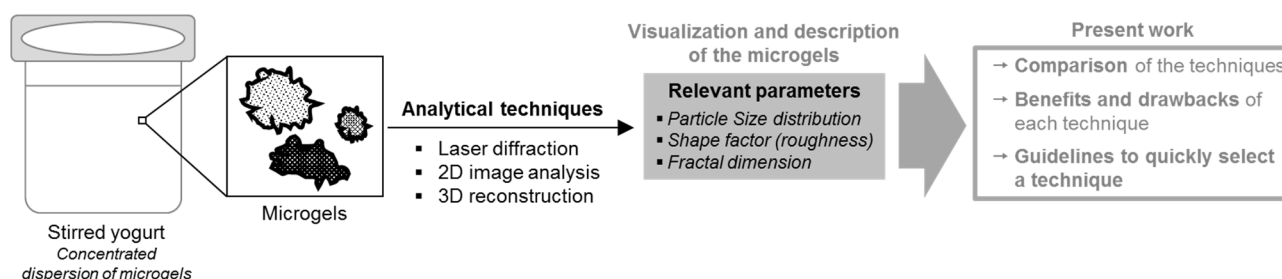
What do stirred yogurt microgels look like? Comparison of laser diffraction, 2D dynamic image analysis and 3D reconstruction

Marine Moussier^a, Valérie Guénard-Lampron^b, Kevin Lachin^a, Gabrielle Moulin^a, Sylvie L. Turgeon^b, Camille Michon^a, Delphine Huc-Mathis^a, Véronique Bosc^a

^a*Ingénierie Procédés Aliments, AgroParisTech, Inra, Université Paris-Saclay, 91300 Massy, France*

^b*Dairy Science and Technology Research Centre (STELA), Institute of Nutrition and Functional Foods (INAF), Université Laval, Quebec City, Qc, G1V 0A6, Canada*

Graphical abstract



Highlights

- Microgel size distributions were similar using LD, 2D and 3D techniques.
- Microgels were non-spherical, rough and heterogeneous with the 2D and 3D analyses.
- Estimations of the fractal dimension were more reliable using LD and 3D than 2D.
- LD was relevant, fast and versatile in accessing size and fractal dimension.
- 2D was faster and 3D more accurate in accessing both shape and fractal dimension.

Abstract

Stirred yogurts can be considered as concentrated dispersions of microgels. The size, shape and fractal dimension of these microgels are known to have a direct impact on textural and sensory properties of stirred yogurts, consequently their thorough characterization is of interest. Different techniques can be used including laser diffraction (LD), 2D dynamic image analysis or 3D reconstruction from z-stack confocal images. The aim of this study was to compare the ability of the three techniques to describe the size, shape and fractal dimension of the stirred yogurt microgels. Two stirred yogurts with different compositions, one fat free (0.1 %) and one high fat (9.3 %), were used. The microgel size distributions obtained were similar using LD, 2D image analysis and 3D reconstruction. Additionally, 2D image analysis and 3D reconstruction enabled visualization of the microgels and access to their shape through morphological factors such as roughness index. The microgels observed were non-spherical, rough and heterogeneous in shape. All three techniques also made it possible to determine the fractal dimension of the microgels, but 2D image analysis displayed lower values than LD and 3D reconstruction.

Keywords

Size, Shape; Stirred yogurt microgels; Laser diffraction; 2D dynamic image analysis; 3D reconstruction.

31 **1. Introduction**

32 From a structural point of view, stirred yogurts are concentrated dispersions of microgels (soft
33 particles) whose diameters range from 10 to 100 μm (Sodini, Remeuf, Haddad, & Corrieu, 2004; Van Marle,
34 1998). In presence of fat, each microgel can itself be considered as an emulsion-filled gel, with fat dispersed
35 as droplets that interact with the protein network via the interface located on the surface of fat globules and
36 mainly composed of milk proteins. The term "microgels" is used for the entities obtained after the set yogurt
37 is stirred. Structurally speaking, these microgels are "aggregates" of primary particles of fat droplets and
38 proteins (mainly whey protein / casein micelle complexes). It is established that stirring causes profound
39 changes in the textural and sensory properties of the yogurts by breaking the continuous gel (*i.e.* set yogurt)
40 into microgels (soft particles) (Cayot, Schenker, Houz , Sulmont-Ross , & Colas, 2008; Lee & Lucey,
41 2006). (Shewan & Stokes, 2013) have also demonstrated that the properties of soft particle concentrated
42 dispersions are directly impacted by the properties of the dispersed particles (microgels in the case of stirred
43 yogurts): their hardness, size distribution or shape. Having access to reliable data on particle size distribution
44 (PSD), the distributions of shape factors and average mass fractal dimension of the microgels is thus of
45 interest to understand the textural properties of stirred yogurts.

46 Laser diffraction (LD) particle size analysis (or static light scattering) is commonly used to access the
47 size distribution of stirred yogurt microgels (Chung, Degner, & Julian, 2014; Hahn, Sramek, N bel, &
48 Hinrichs, 2012; Huc, Michon, Bedoussac, & Bosc, 2016; N bel et al., 2016). This technique measures
49 particles ranging from 0.02 to 2,000 μm in diameter. To do so, a laser beam of known wavelength ($\lambda = 633$
50 nm) irradiates the suspension to be analyzed, and detectors located at specific angles collect the intensity of
51 the light scattered by the particles. Assuming spherical particles with homogenous composition, the software
52 then uses the Mie theory to deduce a theoretical PSD from the light scattering results obtained with LD. To
53 successfully use the Mie theory, knowledge of the refractive and absorbance indexes of the dispersed
54 medium is required (Malvern Instruments Ltd., 2007). In the specific case of the stirred yogurt microgels,
55 these optical indexes are difficult to access. The question of the consistency of the LD size measurement of
56 complex systems like stirred yogurt microgels thus naturally arises. As this technique does not enable access
57 to shape, other techniques of image analysis can be used, compared and possibly combined with LD to
58 obtain the most accurate results possible.

59 2D dynamic image analysis is a recently developed technique that enables precise access to the PSD
60 and to the shape of different types of particles (Carugo et al., 2015; Mallipreddi, Saripella, & Neau, 2014;
61 Perez et al., 2017). This technique can be compared to a modern microscope using a pulsed light source and
62 a high speed mega-pixel camera (K hler, St binger, List, & Witt, 2008; List, K hler, Witt, GmbH, &
63 Pulverhaus, 2011). Unlike laser diffraction analysis, image analysis directly records the properties of the
64 image of each particle to determine diameter and shape factors. 2D image analysis thus appears to be an
65 appropriate tool to access data concerning the morphology of stirred yogurt microgels. Many shape factors
66 are described in the literature for non-spherical microgels (convexity, roundness, circularity, sphericity or
67 roughness) and the definitions of these factors depends on the equipment and analytical technique used

68 (Hentschel & Page, 2003; Podczek, 1997; Yan & Su, 2017). However, the roughness index was the most
69 often used, because it is relevant regarding surface heterogeneity.

70 A variety of microscopic techniques are used to assess the microstructure of stirred yogurts
71 (Mortazavian, Rezaei, & Sohrabvandi, 2009). These include transmission electron microscopy (TEM),
72 scanning electron microscopy (SEM) and confocal laser scanning microscopy (CLSM), sometimes
73 associated with image analysis (Torres, Amigo Rubio, & Ipsen, 2012). Both TEM and SEM are high
74 resolution techniques, but sample preparation can be complex and quite expensive. Moreover, structure
75 artefacts due to the sample preparation are very often suspected. CLSM is a low-invasive alternative
76 requiring the staining of the compounds to be observed. In particular, this technique makes it possible to
77 obtain a series of two-dimensional images (x, y) by z-stacking. Using the appropriate software, these images
78 can be compiled and computed into a 3D representation. This technique was recently applied to food systems
79 such as continuous model gels (whey protein isolate/polysaccharide) (van den Berg et al., 2008) or soft apple
80 cells (Leverrier, Moulin, Cuvelier, & Almeida, 2017). However, to the best of our knowledge, CLSM
81 associated with 3D reconstruction has not yet been used to assess the size and shape of the microgels of
82 stirred yogurts.

83 Laser diffraction, 2D dynamic image analysis and 3D reconstruction can also be used to extract
84 information on the structure of the samples by means of the mass fractal dimension (D_f). This structural
85 parameter is closely linked to the concept of fractal geometry (object having a structure independent of the
86 scale of observation) and thus compactness. Fractal geometries were first mathematically introduced by
87 Mandelbrot (1975) in the mid-1970s and later used in the field of colloid and aggregates, thus opening a new
88 way of characterizing the structure of aggregates in terms of occupancy rate and compaction of the structure
89 in the volume of the aggregates (Andoyo, Guyomarc, & Burel, 2015; Mellema, Walstra, van Opheusden, &
90 van Vliet, 2002) or roughness and sphericity of the aggregates (Raper & Amal, 1993; Torres et al., 2012). It
91 has been accepted for many years (Forrest & Witten, 1979) that aggregates can be described as fractal-like
92 structures, meaning their mass scales with a characteristic radius through the use a specific dimension named
93 the mass fractal dimension. Unlike the topological dimension, which is strictly an integer (between 1 and 3),
94 the fractal dimension is usually a non-integer number. The use of accurate fractal dimensions thus makes it
95 possible to replace the conventional sphericity assumptions that can be used in modelling the relationship
96 between structural and textural properties.

97 As LD measurements are the most widely used in the dairy field, but have limitations, the first
98 objective of this study was to analyze its suitability for heterogeneous (in composition) and irregularly
99 shaped systems like microgels. This analyze of reliability was made by comparing the LD results with the
100 ones obtained with 2D image analysis and 3D reconstruction (from confocal images). The other objective
101 was to compare the ability of the three different techniques to provide information on the size, shape and
102 fractal dimension of stirred yogurt microgels. For this purpose, a fat free and a high fat commercial yogurts
103 were selected and diluted in purified water. The size distributions and the fractal dimensions of the microgels
104 were determined using all three techniques, whereas their shape factors (length and roughness index

105 distributions) were determined only using 2D and 3D image analyses. The different results obtained were
106 then compared and analyzed as a function of the technique.

107 **2. Materials and methods**

108 **2.1. Stirred yogurt sampling**

109 Two types of plain stirred yogurts from different commercial brands were purchased in the market.
110 *Perle de Lait* (Yoplait, France) was chosen for its high fat (F) content and its classic protein (P) content (9.3
111 g/100g fat, 3.2 g/100g protein). *Taillefine Le Brassé 0%* (Danone, France) was selected because it is fat free
112 and has a quite high protein content (0.1 g/100g fat, 4.5 g/100g protein). For the rest of the study, the stirred
113 yogurt samples are referred as FP3 for *Perle de Lait* and P4.5 for *Taillefine Le Brassé 0%*. **FP3 and P4.5**
114 **were chosen to have a similar aging time (based on their similar expiration dates). They were stored in the**
115 **same conditions (i.e. at 4 °C). All the measurements were performed on two consecutive days.** Purified water
116 used for the dilutions was obtained using a Milli-Q purification system (Millipore, Merck, Germany). It was
117 checked and proved that the level of dilution did not have a significant impact on the results. To achieve
118 good sampling and homogeneity, each yogurt was gently mixed using a small spoon rotated 4 times from the
119 bottom of the pot towards the top, with a quarter turn between each movement. For this study, three dilutions
120 were performed from different pots of a same batch of FP3 and of P4.5.

121

122 **2.2. Laser diffraction analysis**

123 Stirred yogurts were diluted 1:10 (w/w) with purified water in a 100 mL pot and the microgels were
124 dispersed by reversing the pot several times. Size distributions were measured by laser diffraction with a
125 MasterSizer 2000 (Malvern Instruments, UK). To achieve a constant level of obscuration, only some drops
126 of 1:10 diluted stirred yogurts were poured in dispersant tank for the measurement (three repetitions),
127 resulting in a total dilution of 1:100. A refractive index of 1.33 for water and 1.46 for the microgels
128 (refractive index of milk proteins), and an absorption index of 0.01 for the microgels were used (Huc et al.,
129 2016). Several data were deduced from the PSD (Malvern Instruments Ltd., 2007): size volume distribution,
130 particle sizes representing less than 10% ($d(0.1)$, μm), 50% (median diameter $d(0.5)$, μm) and 90% ($d(0.9)$,
131 μm) of the sample, volume ($D[4,3]$, μm) and surface (Sauter mean diameter $D[3,2]$, μm) weighted mean
132 diameters ($D[m,n]$, Eq. 1) and width of the distribution (span, Eq. 2).

$$D[m, n] = \left[\frac{\sum \text{volume}_i \times d_i^{m-3}}{\sum \text{volume}_i \times d_i^{n-3}} \right]^{\frac{1}{m-n}} \quad \text{Eq. 1}$$

$$\text{span} = \frac{d(0.9) - d(0.1)}{d(0.5)} \quad \text{Eq. 2}$$

133 In addition, it was also possible to extract the fractal dimension of the microgel aggregates from the
134 scattering data. The light scattered by porous aggregated structures entails more modeling complexity than

135 the scattering of solid homogenous spheres. One way to overcome this problem is to use the Rayleigh-Gans-
 136 Debye theory (Gregory, 2009; Sorensen, 2001). Assuming the primary particles that comprise the aggregate
 137 behave like Rayleigh scatterers (*i.e.* the diameter of the initial particles is much smaller than the wavelength
 138 of the incident beam λ), it is possible to introduce a structure factor $S(q)$ in the expression of the light
 139 scattered intensity $I(q)$ so that (Eq. 3):

$$I(q) \propto S(q) * P(q) \quad \text{Eq. 3}$$

140 where $P(q)$ is the form factor and is due to primary particles. q (m^{-1}) is the scattering vector and is expressed
 141 by Eq. 4, where θ is the scattering angle and n the refractive index of the dispersing medium.

$$q = 4\pi \frac{n}{\lambda} \sin\left(\frac{\theta}{2}\right) \quad \text{Eq. 4}$$

142 As q^{-1} represents the characteristic length probed with the light scattering measurement, information
 143 on the aggregate structure can only reasonably be extracted for q^{-1} values so that $r_0 \ll q^{-1} \ll R_{ag}$, where r_0
 144 denotes the characteristic size of the primary particles, and R_{ag} (m) the characteristic size of the aggregates.
 145 Under this condition, the structure factor depends on the fractal dimension, and it is thus possible to write the
 146 proportionality relation between the intensity of the light scattered and the structure factor as stated by Eq. 5.

$$I(q) \propto q^{-D_f} \quad \text{Eq. 5}$$

147 Using a Log-Log scale plot, it was thus possible to access the mean mass fractal dimension of the
 148 sample by simply determining the slope of the scattering plot in the above-mentioned q^{-1} region (see Fig. 5
 149 in Supplementary material). This theory has been successfully applied in several studies involving colloidal
 150 suspensions, particularly latexes, well calibrated in size and shape (Burns, Yan, Jameson, & Biggs, 1997;
 151 Lachin et al., 2017; Selomulya, Amal, Bushell, & Waite, 2001). More closely connected with the food and
 152 dairy industries, some successes have been achieved in the light scattering study of model casein and
 153 micellar casein aggregates (Chardot, Banon, Misiuwianiec, & Hardy, 2002; Panouillé, Durand, Nicolai,
 154 Larquet, & Boisset, 2005; Vétier, Banon, Chardot, & Hardy, 2003).

155 2.3. 2D dynamic image analysis

156 Dynamic image analysis was performed using a QICPIC/R modular particle size and shape analyzer
 157 and a LIXELL wet dispersing unit (Sympatec GmbH, DE). A precision M4 lens measuring from 1 to 750 μm
 158 with a 0.5 mm cuvette was used. Stirred yogurts were diluted 1:2000 (*w/w*) with purified water in a 1000 mL
 159 beaker to disperse the microgels and the dispersed microgels were then stirred at 100 rpm for 1 min and
 160 pumped into the dispersing unit with a peristaltic pump (Masterflex L/S Model 77201-60, Cole-Parmer, FR)
 161 at a flow rate of 25 mL/min. For each dilution, two 30-second image acquisitions were performed at 10 Hz.
 162 The images were processed using PAQXOS application software (PAQXOS, Version 2.2.2, Sympatec
 163 GmbH, DE). Size measurement data such as volume distribution, $d(0.1)$, $d(0.5)$, $d(0.9)$, $D[4,3]$ and $D[3,2]$
 164 were retrieved from the image analysis. The diameters of the equivalent surface circle of microgels and
 165 maximum (F_{max} , μm) and minimum (F_{min} , μm) Feret diameters, derived respectively using the maximum and

166 minimum distance between two tangents of the contour of the particle, were determined by the software. The
167 width of the distribution (span) was calculated by Eq. 2. The software was also able to determine shape
168 factors including the roughness index (Eq. 6).

$$\text{roughness (2D)} = \frac{\text{perimeter of equivalent circle}}{\text{real perimeter}} \quad \text{Eq. 6}$$

169
170 The results of the dynamic image analysis made it possible to measure fractal dimensions. Some
171 studies have already proposed methods of calculating two-dimensional fractal dimensions (D_2) from image
172 analysis (Jiang & Logan, 1991; Serra & Casamitjana, 1998). The two-dimensional fractal dimension was
173 determined by the relationship between the area (A) of the microgels and their maximum Feret diameter
174 (F_{max}) (Eq. 7). In the specific case of the calculation of the two-dimensional fractal dimensions, the microgels
175 below 10 μm in diameter were not selected due to their low image resolution (1 μm = 1 pixel). For each
176 yogurt analysis, 7,000 microgel images were randomly selected and classified according to their roughness
177 index. For each class of roughness, a plot $\text{Log}(A)$ vs. $\text{Log}(F_{max})$ was performed. A weighted average of these
178 classes was performed to determine a representative D_2 value of all measured stirred yogurts.

$$A \propto F_{max}^{D_2} \quad \text{Eq. 7}$$

179
180 Using simulated aggregates, Lee & Kramer (2004) found a relationship between the two-dimensional
181 fractal dimension (D_2) obtained from image analysis and the three-dimensional fractal dimension (D_3) from
182 the laser diffraction results (Eq. 8). The equation was validated by comparing experimental D_3 (laser
183 diffraction and electrical sensing) with simulated D_3 on different particles, particularly spherical ones
184 (Baalousha, Manciulea, Cumberland, Kendall, & Lead, 2008; Lee & Kramer, 2004).

$$D_3 = 1.391 + 0.01e^{2.164D_2} \quad \text{Eq. 8}$$

185 **2.4. 3D reconstruction from confocal images**

186 **2.4.1. Acquisition by confocal microscopy and 3D processing**

187 The stirred yogurts were first diluted 1:100 (w/w) with purified water in a 100 mL pot, and the
188 microgels were then gently dispersed by reversing the pot several times. The proteins that made up the
189 microgels were then stained by mixing 250 μL of this solution with 2.5 μL of DyLight 488 nm (Thermo
190 Fisher Scientific, Waltham, MA, USA) (one repetition per dilution). Confocal images were acquired with a
191 TCS SP8 AOBS inverted confocal laser scanning microscope (CLSM) (Leica, Solms, Germany) equipped
192 with a Helium-Neon laser (458 nm excitation wavelength) and an Argon laser (633 nm excitation
193 wavelength). From 93 to 195 images (x,y) were acquired by z -scan (0.8 μm steps) with a magnification $\times 40$.
194 For each sample, the z -stacks obtained were combined and processed to reconstitute the 3D microgels using
195 Scan IP™ software (version 7.0, build 2656, © 2000–2014 Simpleware Ltd.). The different processing steps
196 are based on the work of Leverrier et al. (2017) and are illustrated in Fig. 1. The 2D confocal images (x, y) of

197 each z-series were first combined into a 3D reconstruction. A median filter was then applied to the
 198 background of the images (neighborhood radius of $1 \times 1 \times 1$ pixel) to eliminate noise. By comparison with
 199 the initial confocal images, a threshold was eventually chosen to select the level of grey that differentiated
 200 the stained microgels from the background. The 3D reconstitutions shown here were chosen as being
 201 representative of the replications.

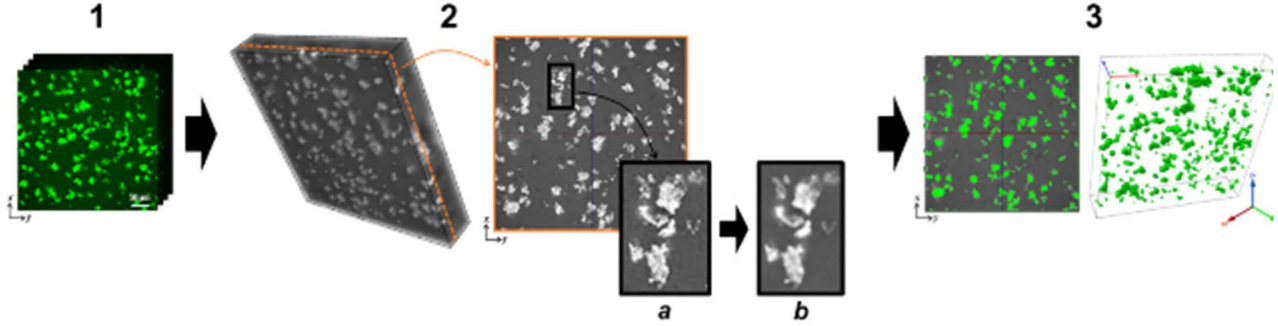


Fig. 1 Processing steps used to reconstitute the 3D microgels of stirred yogurt: **1)** z-acquisition of 2D confocal images (x, y) (proteins in green); **2)** 3D reconstruction and application of a median filter (**a** \rightarrow **b**); **3)** 3D identification of the microgels.

2.4.2. Data computation from 3D reconstruction

202
 203 From the 3D reconstructions, Scan IPTM software provided several data on both size and shape, some
 204 of which were either recovered or processed in this study. First, the software provided the number of
 205 individual microgels identified in the 3D reconstruction and their corresponding volume (μm^3). In order to
 206 obtain the size distribution of the microgels in equivalent sphere, their volumes were discretized (logarithmic
 207 scale). To ensure good quality discretization, at least eight classes were required to plot each distribution (*i.e.*
 208 with volume fractions greater than 0%), with a minimum of two classes per decade. Like with laser
 209 diffraction, $d(0.1)$ (μm), $d(0.5)$ (median diameter, μm), $d(0.9)$ (μm), $D[3,2]$, $D[4,3]$ and span were retrieved
 210 from the reconstituted size distribution. From the volume of each microgel, their equivalent sphere diameter
 211 (Eq. 9) then the surface of their equivalent sphere (Eq. 10) were calculated. A roughness index of the
 212 microgels was calculated by dividing the surface of an equivalent sphere by the real surface (μm^2) given by
 213 the software (Eq. 11). For each microgel, the volumes of the oriented bounding ellipsoid and the
 214 corresponding minor, medial and major lengths (μm) were also obtained using the same software. The
 215 distributions of the roughness index, minor length and major length were plotted by discretizing the data
 216 (using the volume of equivalent sphere).

$$\text{equivalent sphere diameter } (\mu\text{m}) = \sqrt[3]{\frac{6 \times \text{volume}}{\pi}} \quad \text{Eq. 9}$$

$$\text{surface of equivalent sphere } (\mu\text{m}^2) = \pi \times \left(\sqrt[3]{\frac{6 \times \text{volume}}{\pi}} \right)^2 \quad \text{Eq. 10}$$

$$\text{roughness (3D)} = \frac{\text{surface of equivalent sphere}}{\text{real surface}} \quad \text{Eq. 11}$$

217

218 It was also possible to use the data provided by the 3D processing to estimate the mean fractal
 219 dimension of the sample concerned. By definition of the fractal scaling, the mass of a fractal aggregate m_{ag}
 220 (kg) composed of initial particles of radius r_0 (m) and mass m_0 (kg) can be linked to the characteristic cluster
 221 size R_{ag} so that (Bushell, Yan, Woodfield, Raper, & Amal, 2002; Gregory, 2009; Lazzari, Nicoud, Jaquet,
 222 Lattuada, & Morbidelli, 2016) (Eq. 12):

$$n_p = \frac{m_{ag}}{m_0} = k_0 \cdot \left(\frac{R_{ag}}{r_0} \right)^{D_f} \quad \text{Eq. 12}$$

223 where n_p stands for the original number of particles in the aggregate. The radius of gyration is often taken as
 224 the characteristic aggregate size. However, as mentioned by Lazzari et al. (2016), any characteristic length of
 225 the aggregate can be used instead. The shape of the relation remains identical, but the effective value of k_0
 226 changes. The effective density ρ_e of a fractal aggregate (taking its porosity into account) is proportional to
 227 R_{ag} as presented by Eq. 13 (Gregory, 2009):

$$\rho_e \propto R_{ag}^{3-D_f} \quad \text{Eq. 13}$$

228
 229 The 3D reconstruction did not allow the determination of the mass of each single aggregate. However,
 230 it provided values for the volume of each aggregate V_{ag} (m³) and its surface envelope S_{ag} (m²). In this study,
 231 it was chosen to use the ratio V_{ag}/S_{ag} as the characteristic length of the aggregates. By combining the two last
 232 mentioned relations (Eq. 12 and Eq. 13), it was then possible to find a proportionality relation between the
 233 volume of the aggregates and its volume-over-surface ratio so that (Eq. 14):

$$V_{ag} \propto \left(\frac{V_{ag}}{S_{ag}} \right)^{D_f/3-D_f} \quad \text{Eq. 14}$$

234
 235 Thus, by plotting $\text{Log}(V_{ag})$ vs. $\text{Log}(V_{ag}/S_{ag})$ (see Fig. 5 in Supplementary material) for all the stirred
 236 yogurt microgels, and extracting the slope of the linear correlation, it was possible to estimate the average
 237 mass fractal dimension of the microgels.

238 2.5. Statistical analysis

239 Statistical analyses were performed using XLSTAT 2015.1 software (Addinsoft, Paris, France).
 240 Analysis of variance (ANOVA) was used to evaluate differences between values using Tuckey's test. A
 241 significance level of $p < 0.05$ was used.

242 3. Results and discussion

243 The size distribution, shape and fractal dimension of the stirred yogurt microgels were measured using
 244 the three techniques (laser diffraction and/or 2D image analysis and 3D reconstruction) and are reported in
 245 the following tables and figures in order to evaluate the suitability, advantages and limitations of the three
 246 techniques. The two stirred yogurts (FP3 and P4.5) are rarely compared since they are intentionally chosen
 247 as being different to compare techniques in two systems representative of the variety of stirred yogurt
 248 microstructures.

249 3.1. Comparison of microgel size distributions (LD, 2D, 3D)

250 Fig. 2 shows the size distributions obtained using the three measurement techniques and, below, some
 251 data that are characteristic of these distributions. For both FP3 (Fig. 2 A) and P4.5 stirred yogurts (Fig. 2 B),
 252 the distributions obtained by laser diffraction, 2D image analysis and 3D reconstruction were all unimodal
 253 and rather overlapped for a given stirred yogurt. The FP3 microgels were smaller than those of the P4.5
 254 stirred yogurt, with a median size between 10 and 16 μm for FP3 and between 17 and 24 μm for P4.5. These
 255 results mainly indicate that the three techniques are consistent. Moreover, the orders of magnitude of the
 256 obtained sizes are in accordance with measurements made by some authors who used laser diffraction or
 257 CLSM for different stirred yogurts (Cayot et al., 2008; Hahn et al., 2015; Huc et al., 2016). The differences
 258 between the two stirred yogurts (Fig. 2 A and B) were certainly mainly due to their composition and their
 259 stirring process, which are known to have the most impact on microgel size (Mokoonlall, Nöbel, & Hinrichs,
 260 2016; van Marle, van den Ende, de Kruif, & Mellema, 1999).

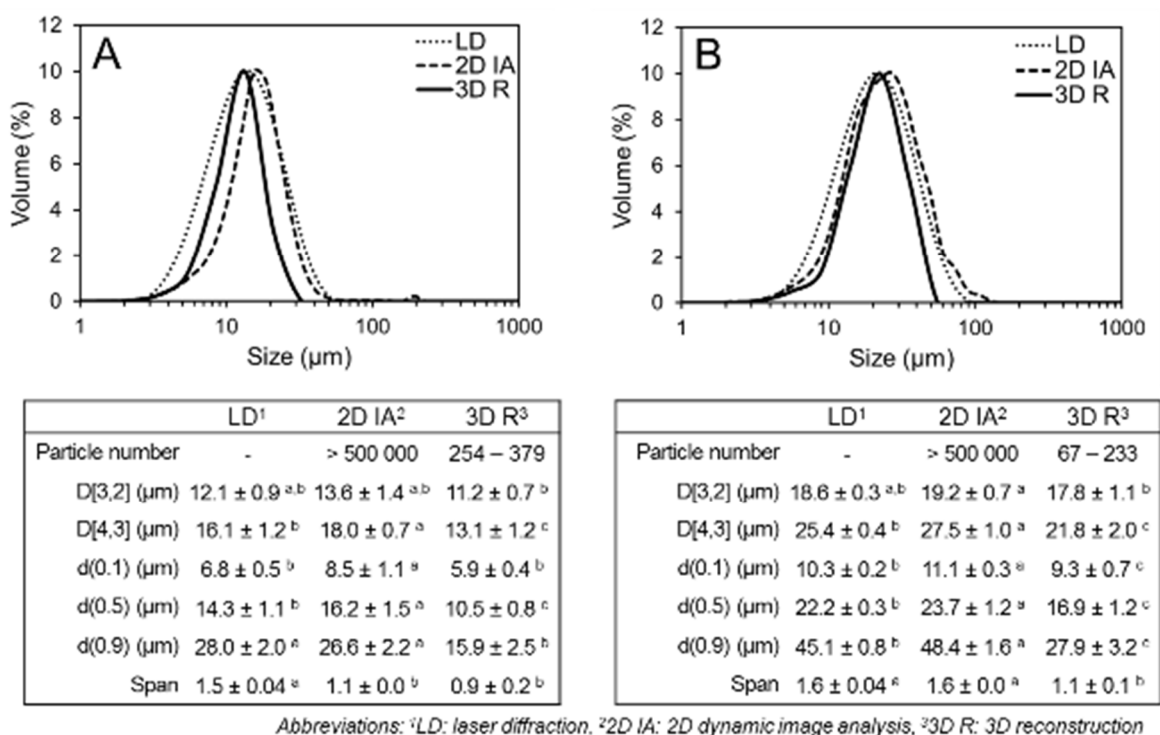


Fig. 2 Size distributions obtained using laser diffraction (dotted lines), 2D dynamic image analysis (dashed lines) and 3D reconstruction (solid line). The tables give the diameters and descriptive parameters corresponding to the different size distributions. The table on the left shows data for the FP3 microgels (A) and the table on the right shows data for the P4.5 microgels (B). Values with different letters in the same row differ significantly at $p < 0.05$.

261
 262 Although unimodal and in the same size ranges (similar order of magnitude), the distributions
 263 obtained also showed some differences depending on the measurement technique used, mainly for bigger
 264 sizes. For the FP3 stirred yogurt (Fig. 2 A), the LD measurement displayed the broadest distribution resulting
 265 in a significantly higher span. The size distributions obtained from 2D image analysis and 3D reconstruction
 266 had similar spans, but the 2D sizes were significantly bigger (d(0.5), d(0.9), D[4,3]). For the P4.5 stirred
 267 yogurt (Fig. 2 B), the 3D distribution differed from that of the LD and 2D distributions, in particular by
 268 being significantly narrower (smaller span) and by displaying fewer big microgels (smaller d(0.9) and

269 D[4,3]). Several authors also reported that the size distributions differed with the technique used when the
270 particles were non-spherical particles. Yu & Hancock (2008) showed that the LD size distributions of
271 elongated microcrystalline cellulose particles (150-250 μm) were wider than their 2D distributions measured
272 by dynamic image analysis. Califice et al. (2013) demonstrated that 2D dynamic image analysis tended to
273 overestimate/underestimate the size of non-spherical particles (50-500 μm elongated metallic particles)
274 compared to 3D reconstruction values obtained from X-ray microtomography images. The literature
275 explained the differences in size distributions by both the measurement technique and the method of
276 calculation used (Califice et al., 2013; Köhler et al., 2008; Tinke et al., 2008; Yu & Hancock, 2008). In the
277 present study, LD hypothesized that the particles analyzed were spherical. The calculation of the 2D
278 diameter corresponded to the diameter of a circle of equal projection area (EQPC) and depended on the
279 orientation of the microgel when measured. With 3D reconstruction, the measurement was protein-specific
280 (CLSM staining) and the calculated diameter corresponded to the diameter of the equivalent sphere in
281 volume (and did not depend on the orientation of the microgel). All these differences between the techniques
282 likely explain the slight discrepancies shown in Fig. 2 for each of the stirred yogurts and suggest their
283 microgels were not spherical. Further analysis of the microgel shape was thus performed to better understand
284 the differences in size distribution, to compare the techniques and to characterize the stirred yogurt microgels
285 more precisely.

286 3.2. Comparison of the shape of the microgels (2D, 3D)

287 2D image analysis and 3D reconstruction were both used to determine the microgel shape. Fig. 3 A
288 illustrates how the characteristic lengths were obtained from 2D (F_{max} and F_{min}) and 3D (major and minor)
289 analyses. Fig. 3 B(a) and C(a) below show the distributions of the different lengths for FP3 and P4.5 stirred
290 yogurts, respectively. These length distributions are classically used to provide information about the shape
291 (spherical or elongated) of the particles (Califice et al., 2013; Yu & Hancock, 2008). When microgels are
292 spherical, the maximum length is obviously the same as the minimum length (Yu & Hancock, 2008). Here,
293 minor and F_{min} length distributions were smaller than major and F_{max} distributions for FP3 and P4.5,
294 indicating that stirred yogurt microgels are not spherical, as previously suspected based on differences in size
295 distributions obtained with the LD, 2D dynamic image analysis and 3D reconstruction. These results are in
296 agreement with the fresh cheese microgels observed by Hahn et al. (2014) using CLSM, which were also
297 irregular in shape. In addition, the P4.5 length distributions obtained from the 2D image analysis were
298 broader than those obtained from 3D reconstruction. The differences between the 3D lengths (i.e. between
299 minor and major) were more important than the differences between the 2D lengths (i.e. between F_{min} and
300 F_{max}). These results reveal some differences between the 2D and 3D distributions that can mainly be
301 explained by the way the lengths were obtained with each technique (Fig. 3 A). From the 2D image analysis,
302 F_{min} and F_{max} lengths could be biased by the orientation of microgels when measured (orientated lengthwise
303 due to the flow). A similar concern has been expressed for irregular concrete aggregates (Cepuritis,
304 Garboczi, Jacobsen, & Snyder, 2017). With 3D reconstruction, the microgel may not be in direct contact
305 with the ellipsoid edge to encompass the entire microgel (in length, width and thickness) (Fig. 3 (A)). This

306 technique may therefore overestimate the minor and major lengths. Based on X-ray microcomputed
 307 tomography, [Cepuritis et al. \(2017\)](#) reported that 3D minor and major lengths depended on the dimension of
 308 the rectangular box enclosing the particle. In addition, in the present study, there were more differences
 309 between the two techniques for the P4.5 stirred yogurt. This result showed that P4.5 stirred yogurt microgels
 310 are more heterogeneous in shape (with more different types of elongation) than FP3 ones.

311 Images (b) and (c) in [Fig. 3 B](#) and [C](#), show the stirred yogurt microgels obtained using 3D
 312 reconstruction (from the z-stack confocal images) and 2D images analysis, respectively, confirming that the
 313 microgels were very heterogeneous in size and shape. This is in agreement with the results of [Hahn et al.](#)
 314 [\(2015\)](#), who observed CLSM images of fresh cheese under different processing conditions. 2D images of
 315 FP3 and P4.5 stirred yogurts also showed different degrees of microgel compactness ([Fig. 3 \(c\)](#)). For
 316 example, the enlarged #1 microgels obtained from the screenshots (2D image analysis) appear to be more
 317 compact than the #2 ones ([Fig. 3 B \(c\)](#) and [Fig. 3 C \(c\)](#)).

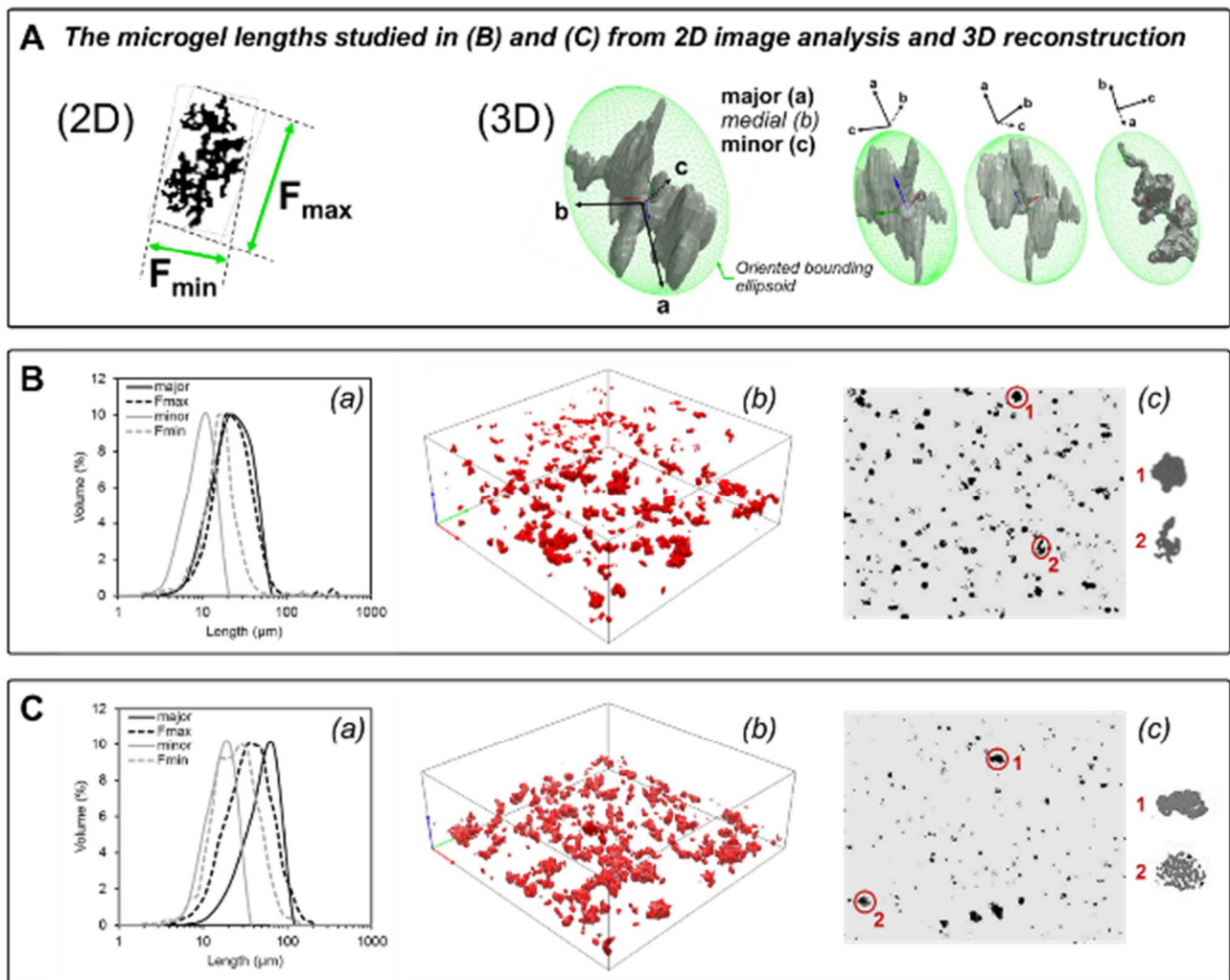


Fig. 3 Details of microgel lengths (major, F_{max} , minor, F_{min}) (A) studied for FP3 (B) and P4.5 (C) stirred yogurts through: (a) the length distributions (average curves) obtained from 2D image analysis (dashed lines) and 3D reconstruction (solid lines), (b) the 3D reconstructions and (c) a screenshot of the movie processed throughout 2D image analysis.

318

319 Fig. 4 presents the roughness index distributions obtained for FP3 (A) and P4.5 (B) stirred yogurts.
320 The roughness index value ranges from 0 to 1 and describes the surface unevenness on the microgels. The
321 index tends towards 1 for microgels with no unevenness (*i.e.* a smooth circle (2D) or sphere (3D)).

322 For each technique considered independently, the roughness distributions of the two stirred yogurts
323 were globally similar, even if that of P4.5 was slightly broader. The differences in the yogurt compositions
324 and stirring processes could explain this slight difference in roughness distributions. However, there were
325 bigger differences between the 2D and 3D roughness distributions. Using 3D reconstruction, the distributions
326 were narrow and unimodal, with a median roughness of 0.8, whereas using 2D images analysis, they
327 displayed a main peak with a shoulder, with a first peak at 0.6 and a second one at 0.8-0.9. The 2D
328 distributions were also broader (from 0.2-0.3 to 1) than 3D ones (0.4-0.5 to 1). These results indicate that the
329 stirred yogurt microgels appears less uniform in roughness with 2D images analysis. The difference could be
330 explained by the processing steps used to reconstitute the 3D microgels. The application of a median filter
331 and the selection of a threshold (subsection 2.4.1 and Fig. 1) could smooth the microgel surfaces (*i.e.* the
332 boundary between the background and the microgels) and therefore underestimate the width of the roughness
333 distributions.

334 Although these microgels tended towards a smooth surface (roughness mostly between 0.7 and 0.8),
335 the range of widths of the distribution underlined the heterogeneity of the stirred yogurt microgels that can be
336 linked to microgel size. Some studies already linked the shape of the particles such as the roughness index, to
337 their size (Yan & Shi, 2014; Zhou & Wang, 2017). In the present study, the roughness index decreased (*i.e.*
338 surface unevenness was greater) in bigger microgels (data not shown). Rougher microgels are probably due
339 to the bigger size ($> 30 \mu\text{m}$) of microgels that were mostly measured using 2D analysis rather than 3D
340 reconstruction (subsection 3.1).

341

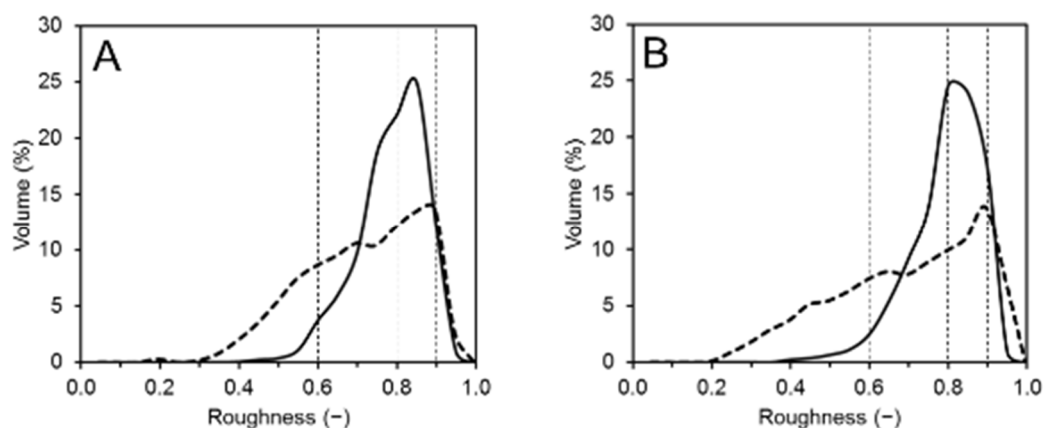


Fig. 4 Weighted average curves (three repetitions) of the roughness index distributions obtained from 2D image analysis (dashed lines) and 3D reconstruction (solid lines) for FP3 (A) and P4.5 (B) stirred yogurts.

342 3.3. Comparison of the microgel fractal dimension (LD, 2D, 3D)

343 All three techniques were used to estimate the microgel fractal dimension of the two stirred yogurts
344 (FP3 and P4.5). For the LD measurements, the slopes were extracted with very high regression coefficients
345 (higher than 0.99). For 3D reconstruction, the linear regression also proved to be very high, with values

346 systematically higher than 0.96. With 2D dynamic image analysis, the two-dimensional fractal dimensions
 347 (D_2) were also extracted with very high regression coefficients, *i.e.* higher than 0.91. These high values
 348 indicated excellent fitting, thus allowing high confidence in the results obtained using these techniques
 349 (Table 1).

350 **Table 1** Average fractal dimensions obtained from laser diffraction, 2D image analysis and 3D reconstruction. Values
 351 with different letters in the same column differ significantly at $p < 0.05$.

Technique	FP3	P4.5
Laser diffraction	2.31 ± 0.01 <i>a</i>	2.37 ± 0.03 <i>a</i>
2D image analysis	2.05 ± 0.02 <i>c</i>	2.08 ± 0.02 <i>c</i>
3D reconstruction	2.26 ± 0.01 <i>b</i>	2.27 ± 0.03 <i>b</i>

352
 353 The average of the mass fractal dimensions (D_f) obtained from LD and 3D reconstruction were similar
 354 even if significantly different, with values around 2.3 for the two samples. These values are in good
 355 agreement with values reported in the literature for fermented stirred milk gels (van Marle et al., 1999). In
 356 conventional studies on Brownian aggregation of particles (generally latex suspensions), the obtained D_f
 357 values are discussed in the frame of two limiting regimes. Such studies are conducted under low volume
 358 concentrations during aggregation (typically $10^{-3} - 10^{-4}$ %), ensuring the validity of the theory. When there is
 359 no energy barrier between the colliding particles, each collision leads to aggregation. This regime is called
 360 “diffusion limited aggregation” (DLA) and results in loose open structures with D_f around 1.7 – 1.8. When
 361 the repulsion forces are still significant, the particles can penetrate the aggregate structure before adhering.
 362 This regime is called “reaction limited aggregation” (RLA) and leads to denser aggregates, with D_f around
 363 2.1. In the present study, the volume fractions of milk proteins (before any dilution) were higher than 1% in
 364 both stirred yogurts (FP3 and P4.5), which explains why the values obtained were significantly higher
 365 (Bremer, van Vliet, & Walstra, 1989). In addition, the colloidal calcium phosphate, which ensures the
 366 structure integrity of the casein micelles, dissolves during acidification. This dissolution results in the
 367 loosening of the micelles (increasing their volume), which likely promotes the compaction of the protein
 368 aggregates due to loss of repulsive interactions and thus leads to denser structures (Andoyo et al., 2015).

369 The D_f value calculated from 3D reconstruction could be considered as the most accurate of the three
 370 techniques, because it relies on direct visualization of the aggregates and assumes no strong assumption.
 371 However, the LD technique proved to be a very good alternative technique to obtain D_f as the differences
 372 between LD and 3D were very small. However, the values obtained using 2D image analysis and the
 373 equation proposed by Lee & Kramer (2004) differed more from 3D measurements. Estimating D_f from 2D
 374 image analysis using this equation thus appears to be questionable in the case of stirred yogurt microgels.
 375 Lee & Kramer (2004) reported underestimation of D_f in the case of *E. coli* aggregates and explained that it
 376 was partly because *E. coli* were not spherical, which could also be the case of the stirred yogurt microgels.
 377 The 3D and LD techniques are thus recommended over 2D analysis.

378 **3.4. Comparison of the advantages and limitations of LD, 2D and 3D**

379 To complete the comparison of the performances of the three techniques, [Table 2](#) summarizes the size
 380 distribution range, the measurement conditions, the time needed for measurement and data treatment per
 381 sample, the properties obtained directly or calculated from the data as well as the assumptions and
 382 weaknesses.

383 While LD, 2D image analysis and 3D reconstruction proved to be quite consistent in characterizing
 384 stirred yogurt microgels, [Table 2](#) shows that they each had their advantages and limitations. The LD
 385 technique mainly assumes that the analyzed particles are homogeneous and spherical, which has been shown
 386 ([subsection 3.1](#)) to lead to overestimation of the bigger particles and/or underestimation of the smaller
 387 particles when measuring the microgel sizes of the stirred yogurts. Moreover, this technique requires
 388 refractive and adsorption indexes, which can be difficult to estimate for complex systems composed of
 389 different ingredients. However, in the case of the stirred yogurt microgels, these indexes were not
 390 problematic since no variation in the size distribution was observed when their values varied (due to the
 391 sufficiently large size of the microgels). Although LD obviously does not allow access to shape factors, it is
 392 quick and user-friendly for accessing the size distribution and the fractal dimension. It also makes it possible
 393 to measure particles less than a micron in size, which is not the case of the 2D and 3D techniques presented
 394 here (limited by their optical geometry characteristic).

395 **Table 2** Comparison of laser diffraction, 2D image analysis and 3D reconstruction. Information in **bold** indicates the
 396 advantages of each technique.

Technique	Laser diffraction	2D image analysis	3D reconstruction
Equipment	MasterSizer 2000 (Malvern)	QICPIC/R and LIXELL (Sympatec)	CLSM (Leica) and Scan IP™ (Simpleware)
Size range	0.02 to 2,000 μm	1 to 750 μm (M4 lens)	0.532 μm (<i>i.e.</i> pixel) to a few millimeters
Measurement conditions	Dilution 1:100, Agitation, Pumping	Dilution 1:2000, Agitation, Pumping	Dilution 1:100, Staining
Measuring time per sample	10 min	30 sec	30 min
Time needed for data treatment per sample	10 min	30 min	1 h
Properties obtained directly	Size	Size, Shape factors, Visualization of microgel projection (2D)	-
Calculated properties	Fractal dimension	Fractal dimension	Size, Shape factors, Fractal dimension, realistic visualization of the microgels (3D)
Assumptions and limitations	(i) Particles considered as homogeneous and spherical (ii) Need for refractive and absorption indexes (iii) No access to particle shape	(i) Data based on projected areas of the particles (depending on their orientation) (ii) Low camera resolution (iii) Need for low concentrations of particles	(i) Threshold to select pixels of interest (identification of the stained particles) (ii) Small number of particles (iii) Time consuming data processing

397
 398 As mentioned above, 2D dynamic image analysis cannot reasonably measure sizes smaller than 1 μm,
 399 and this needs to be taken into account when studying food structures that can be below this threshold

400 (colloidal systems, for example). The first limitation is that although the mass fractal dimension can be
401 estimated using a specific relation reported in the literature, (subsection 3.3) its use was shown to be
402 questionable in the case of the stirred yogurt microgels. Moreover, the time required to process the data is
403 quite long, and this technique analyzes the projected areas (2D) of the measured particles, which may depend
404 on their orientation during measurement. On the other hand, it has the advantage of allowing a very large
405 number of particles to be analyzed, which should offset the orientation bias. Moreover, it enables relatively
406 rapid measurement and direct access to the size and shape properties. It provided a 2D view of the particles
407 that revealed that the microgels were not spherical, but showed varying degrees of roughness, and were
408 sometimes porous (fractal dimension) in stirred yogurt.

409 The smallest size that can be measured with 3D reconstruction depends on the resolution of the
410 microscope and may be high (*i.e.* allowing to observe small sizes) in food structure analysis. Data acquisition
411 is time consuming and the analysis of the properties of size, shape and fractal dimension requires complete
412 data processing. Moreover, a threshold has to be chosen to select pixels of interest (identification of the
413 stained microgels). The results showed in subsections 3.1, 3.3 and 3.3 demonstrated that the choice made for
414 this study was appropriate in the case of the stirred yogurt microgels studied here. One of the advantages of
415 the 3D technique (using CLSM) is the limited shear undergone by the particles. This is particularly relevant
416 for the study of brittle systems such as stirred yogurt microgels and most food matrices. Based on molecule
417 staining, it also allows the selection of specific compounds within the particles and tailored measurement of
418 the structure. The main strength of 3D reconstruction is that it enables full visualization of the particles, with
419 no orientation bias or sphericity assumption. This specificity was particularly useful in the present study
420 since it offered the opportunity to clearly observe the diverse sizes and shapes of the yogurt microgels.

421 **4. Conclusions**

422 Laser diffraction, 2D dynamic image analysis and 3D reconstruction were shown to be relevant and
423 complementary for the characterization of the size (through PSD), shape and fractal dimension of
424 heterogeneous (in composition) and irregularly shaped systems like stirred yogurt microgels. By comparing
425 LD with 2D image analysis and 3D reconstruction on two different stirred yogurts, we showed that LD was
426 fully relevant to access the size distribution and the mean mass fractal dimension of non-spherical yogurt
427 microgels. The use of 2D dynamic image analysis and 3D reconstruction also raised the question of the
428 characterization of the shape of the stirred yogurt microgels. While rarely used for food systems, 2D
429 dynamic image analysis proved to be advantageous to visualize the microgels and quickly estimate their
430 morphological parameters. 3D reconstruction also has very useful features as it enables access to shape
431 factors while avoiding the possible bias resulting from particle orientation using 2D analysis. However, the
432 3D technique usually entails time consuming sample preparation and analysis, and is thus not really to be
433 recommended for routine analysis. This comparison of the three techniques provides useful guidelines for
434 studying complex food systems. Moreover, these techniques can offer new perspectives to accurately explain
435 the relationship between the microstructure and the macro-scale properties (such as flow properties) of a
436 food system at each step of its processing chain.

438 **Acknowledgements**

439 This work was funded by a single interministerial fund (France) through a collaborative R&D project
 440 certified by Vitagora and Valorial competitiveness clusters as well as by the research programs of the Fonds
 441 de recherche du Québec – Nature et technologies, Novalait Inc., the Ministère de l’Agriculture, des Pêcheries
 442 et de l’Alimentation du Québec (MAPAQ), and the Fondation Famille-Choquette. The authors would like to
 443 thank Philippe Violle, sales manager of Sympatec France, for his help and advice with the dynamic image
 444 analysis processing. The authors also thank Paul Menut and Artemio Plana-Fattori for sharing their
 445 experience and contributing to the development and improvement of this paper.

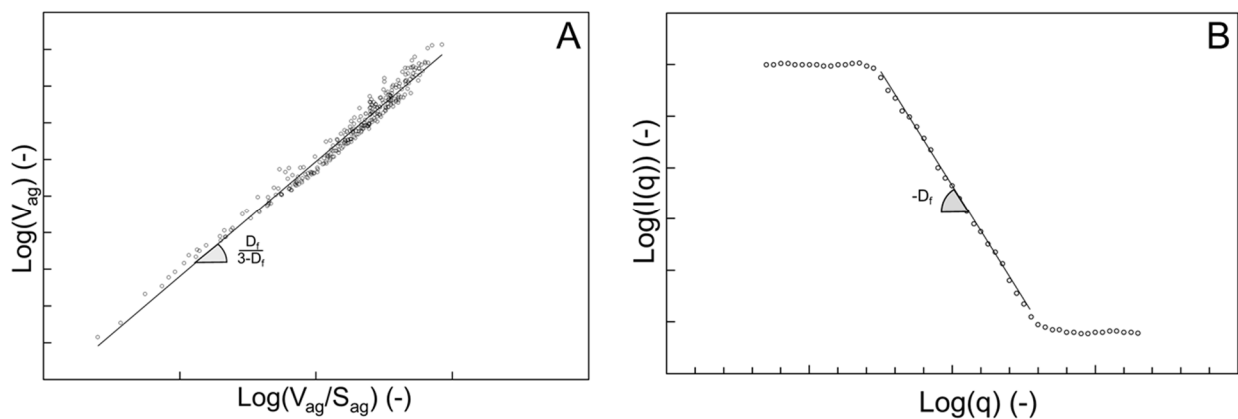
446 **Supplementary material**

Fig. 5 Graph of principle used to obtain the fractal dimension from the laser diffraction data (**A**) and the 3D reconstruction data (**B**) where q (m^{-1}) is the scattering vector, $I(q)$ is the light scattered intensity, V_{ag} (m^3) is the volume and S_{ag} (m^2) the surface envelope of each aggregate.

447 **References**

- 448 Andoyo, R., Guyomarc, F., & Burel, A. (2015). Spatial arrangement of casein micelles and whey protein
 449 aggregate in acid gels: Insight on mechanisms. *Food Hydrocolloids*, *51*, 118–128.
 450 <https://doi.org/10.1016/j.foodhyd.2015.04.031>
- 451 Baalousha, M., Manciuola, A., Cumberland, S., Kendall, K., & Lead, J. R. (2008). Aggregation and surface
 452 properties of iron oxide nanoparticles: influence of pH and natural organic matter. *Environmental*
 453 *Toxicology and Chemistry / SETAC*, *27*(9), 1875–82. <https://doi.org/10.1897/07-559.1>
- 454 Bremer, L. G. B., van Vliet, T., & Walstra, P. (1989). Theoretical and experimental study of the fractal
 455 nature of the structure of casein gels. *Journal of the Chemical Society, Faraday Transactions 1:*
 456 *Physical Chemistry in Condensed Phases*, *85*(10), 3359–3372. <https://doi.org/10.1039/F19898503359>
- 457 Burns, J. L., Yan, Y., Jameson, G. J., & Biggs, S. (1997). A light scattering study of the fractal aggregation
 458 behavior of a model colloidal system. *Langmuir*, *13*(24), 6413–6420. Retrieved from
 459 <http://pubs.acs.org/doi/abs/10.1021/la970303f>
- 460 Bushell, G. C., Yan, Y. D., Woodfield, D., Raper, J., & Amal, R. (2002). On techniques for the measurement
 461 of the mass fractal dimension of aggregates. *Advances in Colloid and Interface Science*, *95*(1), 1–50.
 462 [https://doi.org/10.1016/S0001-8686\(00\)00078-6](https://doi.org/10.1016/S0001-8686(00)00078-6)
- 463 Califice, A., Michel, F., Dislaire, G., & Pirard, E. (2013). Influence of particle shape on size distribution
 464 measurements by 3D and 2D image analyses and laser diffraction. *Powder Technology*, *237*, 67–75.
 465 <https://doi.org/10.1016/j.powtec.2013.01.003>

- 466 Carugo, D., Ankrett, D. N., Zhao, X., Zhang, X., Hill, M., O'Byrne, V., ... Lewis, A. L. (2015). Benefits of
 467 polidocanol endovenous microfoam (Varithena®) compared with physician-compounded foams.
 468 *Phlebology*, 31(4), 283–295. <https://doi.org/10.1177/0268355515589063>
- 469 Cayot, P., Schenker, F., Houzé, G., Sulmont-Rossé, C., & Colas, B. (2008). Creaminess in relation to
 470 consistency and particle size in stirred fat-free yogurt. *International Dairy Journal*, 18(3), 303–311.
 471 <https://doi.org/10.1016/j.idairyj.2007.06.009>
- 472 Cepuritis, R., Garboczi, E. J., Jacobsen, S., & Snyder, K. A. (2017). Comparison of 2-D and 3-D shape
 473 analysis of concrete aggregate fines from VSI crushing. *Powder Technology*, 309, 110–125.
 474 <https://doi.org/10.1016/j.powtec.2016.12.037>
- 475 Chardot, V., Banon, S., Misiuwianiec, M., & Hardy, J. (2002). Growth kinetics and fractal dimensions of
 476 casein particles during acidification. *Journal of Dairy Science*, 85(1), 8–14.
 477 [https://doi.org/10.3168/jds.S0022-0302\(02\)74046-0](https://doi.org/10.3168/jds.S0022-0302(02)74046-0)
- 478 Chung, C., Degner, B., & Julian, D. (2014). Development of Reduced-calorie foods : Microparticulated whey
 479 proteins as fat mimetics in semi-solid food emulsions. *Food Research International*, 56, 136–145.
 480 <https://doi.org/10.1016/j.foodres.2013.11.034>
- 481 Forrest, S. R., & Witten, T. A. (1979). Long-range correlations in smoke-particle aggregates. *Journal of*
 482 *Physics A: Mathematical and General*, 12(5), L109–L117. <https://doi.org/10.1088/0305-4470/12/5/008>
- 483 Gregory, J. (2009). Monitoring particle aggregation processes. *Advances in Colloid and Interface Science*,
 484 147–148, 109–123. Retrieved from <http://linkinghub.elsevier.com/retrieve/pii/S0001868608001462>
- 485 Hahn, C., Müller, E., Wille, S., Weiss, J., Atamer, Z., & Hinrichs, J. (2014). Control of microgel particle
 486 growth in fresh cheese (concentrated fermented milk) with an exopolysaccharide-producing starter
 487 culture. *International Dairy Journal*, 36(1), 46–54. <https://doi.org/10.1016/j.idairyj.2013.12.011>
- 488 Hahn, C., Nöbel, S., Maisch, R., Rösingh, W., Weiss, J., & Hinrichs, J. (2015). Adjusting rheological
 489 properties of concentrated microgel suspensions by particle size distribution. *Food Hydrocolloids*, 49,
 490 183–191. <https://doi.org/10.1016/j.foodhyd.2015.03.020>
- 491 Hahn, C., Sramek, M., Nöbel, S., & Hinrichs, J. (2012). Post-processing of concentrated fermented milk:
 492 Influence of temperature and holding time on the formation of particle clusters. *Dairy Science and*
 493 *Technology*, 92(1), 91–107. <https://doi.org/10.1007/s13594-011-0046-1>
- 494 Hentschel, M. L., & Page, N. W. (2003). Selection of descriptors for particle shape characterization. *Particle*
 495 *and Particle Systems Characterization*, 20(1), 25–38. <https://doi.org/10.1002/ppsc.200390002>
- 496 Huc, D., Michon, C., Bedoussac, C., & Bosc, V. (2016). Design of a multi-scale texture study of yoghurts
 497 using rheology, and tribology mimicking the eating process and microstructure characterisation.
 498 *International Dairy Journal*, 61, 126–134. <https://doi.org/10.1016/j.idairyj.2016.05.003>
- 499 Jiang, Q., & Logan, B. E. (1991). Fractal Dimensions of Aggregates Determined from Steady-State Size
 500 Distributions. *Environmental Science and Technology*, 25(12), 2031–2038.
 501 <https://doi.org/10.1021/es00024a007>
- 502 Köhler, U., Stübinger, T., List, J., & Witt, W. (2008). *Investigations on non-Spherical Reference Material*
 503 *Using Laser Diffraction and Dynamic Image Analysis. Particulate systems analysis.*
- 504 Lachin, K., Le Sauze, N., Di Miceli Raimondi, N., Aubin, J., Gourdon, C., & Cabassud, M. (2017).
 505 Aggregation and breakup of acrylic latex particles inside millimetric scale reactors. *Chemical*
 506 *Engineering and Processing: Process Intensification*, 113, 65–73.
 507 <https://doi.org/10.1016/j.cep.2016.09.021>
- 508 Lazzari, S., Nicoud, L., Jaquet, B., Lattuada, M., & Morbidelli, M. (2016). Fractal-like structures in colloid
 509 science. *Advances in Colloid and Interface Science*, 235, 1–13.
 510 <https://doi.org/10.1016/j.cis.2016.05.002>
- 511 Lee, C., & Kramer, T. A. (2004). Prediction of three-dimensional fractal dimensions using the two-
 512 dimensional properties of fractal aggregates. *Advances in Colloid and Interface Science*, 112(1–3), 49–
 513 57. <https://doi.org/10.1016/j.cis.2004.07.001>
- 514 Lee, W.-J., & Lucey, J. A. (2006). Impact of Gelation Conditions and Structural Breakdown on the Physical

- 515 and Sensory Properties of Stirred Yogurts. *Journal of Dairy Science*, 89(7), 2374–2385.
516 [https://doi.org/10.3168/jds.S0022-0302\(06\)72310-4](https://doi.org/10.3168/jds.S0022-0302(06)72310-4)
- 517 Leverrier, C., Moulin, G., Cuvelier, G., & Almeida, G. (2017). Assessment of deformability of soft plant
518 cells by 3D imaging. *Food Structure*, 14(September), 95–103.
519 <https://doi.org/10.1016/j.foostr.2017.07.002>
- 520 List, J., Köhler, U., Witt, W., GmbH, S., & Pulverhaus, A. (2011). Dynamic Image Analysis extended to Fine
521 and Coarse Particles. *Particulate Systems Analysis*, 1–5.
- 522 Mallipeddi, R., Saripella, K. K., & Neau, S. H. (2014). Use of fine particle ethylcellulose as the diluent in the
523 production of pellets by extrusion-spheronization. *Saudi Pharmaceutical Journal*, 22(4), 360–372.
524 <https://doi.org/10.1016/j.jsps.2013.11.001>
- 525 Malvern Instruments Ltd. (2007). *Mastersizer 2000 - User Manual - MAN0384 Issue 1.0*.
- 526 Mandelbrot, B. (1975). *Les objets fractals, forme, hasard et dimension*. Paris: Flammarion.
- 527 Mellema, M., Walstra, P., van Opheusden, J. H. J., & van Vliet, T. (2002). Effects of structural
528 rearrangements on the rheology of rennet- induced casein particle gels. *Advances in Colloid and*
529 *Interface Science*, 98(1), 25–50.
- 530 Mokoonlall, A., Nöbel, S., & Hinrichs, J. (2016). Post-processing of fermented milk to stirred products:
531 Reviewing the effects on gel structure. *Trends in Food Science and Technology*, 54, 26–36.
532 <https://doi.org/10.1016/j.tifs.2016.05.012>
- 533 Mortazavian, A. M., Rezaei, K., & Sohrabvandi, S. (2009). Application of advanced instrumental methods
534 for yogurt analysis. *Critical Reviews in Food Science and Nutrition*, 49(2), 153–163.
535 <https://doi.org/10.1080/10408390701764807>
- 536 Nöbel, S., Ross, N. L., Protte, K., Körzendörfer, A., Hitzmann, B., & Hinrichs, J. (2016). Microgel particle
537 formation in yogurt as influenced by sonication during fermentation. *Journal of Food Engineering*,
538 180, 29–38. <https://doi.org/10.1016/j.jfoodeng.2016.01.033>
- 539 Panouillé, M., Durand, D., Nicolai, T., Larquet, E., & Boisset, N. (2005). Aggregation and gelation of
540 micellar casein particles. *Journal of Colloid and Interface Science*, 287(1), 85–93.
541 <https://doi.org/10.1016/j.jcis.2005.02.008>
- 542 Perez, M., Décaudin, B., Maiguy-Foinard, A., Barthélémy, C., Lebuffe, G., Storme, L., & Odou, P. (2017).
543 Dynamic Image Analysis to Evaluate Subvisible Particles during Continuous Drug Infusion in a
544 Neonatal Intensive Care Unit. *Scientific Reports*, 7(1), 1–8. [https://doi.org/10.1038/s41598-017-10073-](https://doi.org/10.1038/s41598-017-10073-y)
545 [y](https://doi.org/10.1038/s41598-017-10073-y)
- 546 Podczek, F. (1997). A shape factor to assess the shape of particles using image analysis. *Powder Technology*,
547 93, 47–53.
- 548 Raper, J. A., & Amal, R. (1993). Measurement of aggregate fractal dimensions using static light scattering.
549 *Particle and Particle Systems Characterization*, 10(5), 239–245. Retrieved from
550 [http://onlinelibrary.wiley.com/doi/10.1002/ppsc.19930100505/abstract%5Cnpapers2://publication/uuid/](http://onlinelibrary.wiley.com/doi/10.1002/ppsc.19930100505/abstract%5Cnpapers2://publication/uuid/D7EC2CC6-7FAD-4820-A345-F5985D21E4C4)
551 [D7EC2CC6-7FAD-4820-A345-F5985D21E4C4](http://onlinelibrary.wiley.com/doi/10.1002/ppsc.19930100505/abstract%5Cnpapers2://publication/uuid/D7EC2CC6-7FAD-4820-A345-F5985D21E4C4)
- 552 Selomulya, C., Amal, R., Bushell, G., & Waite, T. D. (2001). Evidence of shear rate dependence on
553 restructuring and breakup of latex aggregates. *Journal of Colloid and Interface Science*, 236(1), 67–77.
- 554 Serra, T., & Casamitjana, X. (1998). Structure of the aggregates during the process of aggregation and
555 breakup under a shear flow. *Journal of Colloid and Interface Science*, 206(2), 505–511.
556 <https://doi.org/10.1006/jcis.1998.5714>
- 557 Shewan, H. M., & Stokes, J. R. (2013). Review of techniques to manufacture micro-hydrogel particles for
558 the food industry and their applications. *Journal of Food Engineering*, 119(4), 781–792.
559 <https://doi.org/10.1016/j.jfoodeng.2013.06.046>
- 560 Sodini, I., Remeuf, F., Haddad, S., & Corrieu, G. (2004). The Relative Effect of Milk Base, Starter, and
561 Process on Yogurt Texture: A Review. *Critical Reviews in Food Science and Nutrition*, 44, 113–137.
562 <https://doi.org/10.1080/10408690490424793>
- 563 Sorensen, C. M. (2001). Light scattering by fractal aggregates : A review. *Aerosol Science and Technology*,

- 564 35(2), 648–687.
- 565 Tinke, A. P., Carnicer, A., Govoreanu, R., Scheltjens, G., Lauwerysen, L., Mertens, N., ... Brewster, M. E.
566 (2008). Particle shape and orientation in laser diffraction and static image analysis size distribution
567 analysis of micrometer sized rectangular particles. *Powder Technology*, 186(2), 154–167.
568 <https://doi.org/10.1016/j.powtec.2007.11.017>
- 569 Torres, I. C., Amigo Rubio, J. M., & Ipsen, R. (2012). Using fractal image analysis to characterize
570 microstructure of low-fat stirred yoghurt manufactured with microparticulated whey protein. *Journal of*
571 *Food Engineering*, 109(4), 721–729. <https://doi.org/10.1016/j.jfoodeng.2011.11.016>
- 572 van den Berg, L., Jan Klok, H., van Vliet, T., van der Linden, E., van Boekel, M. A. J. S., & van de Velde, F.
573 (2008). Quantification of a 3D structural evolution of food composites under large deformations using
574 microrheology. *Food Hydrocolloids*, 22(8), 1574–1583. <https://doi.org/10.1016/j.foodhyd.2007.11.002>
- 575 Van Marle, M. (1998). *Structure and rheological properties of yogurt gels and stirred yogurt*. University of
576 Twente Netherlands.
- 577 van Marle, M. E., van den Ende, D., de Kruif, C. G., & Mellema, J. (1999). Steady-shear viscosity of stirred
578 yogurts with varying ropiness. *Journal of Rheology*, 43(6), 1643–1662.
579 <https://doi.org/10.1122/1.551065>
- 580 Vétier, N., Banon, S., Chardot, V., & Hardy, J. (2003). Effect of Temperature and Aggregation Rate on the
581 Fractal Dimension of Renneted Casein Aggregates. *Journal of Dairy Science*, 86(8), 2504–2507.
582 [https://doi.org/10.3168/jds.S0022-0302\(03\)73844-2](https://doi.org/10.3168/jds.S0022-0302(03)73844-2)
- 583 Yan, W. M., & Shi, Y. (2014). Evolution of grain grading and characteristics in repeatedly reconstituted
584 assemblages subject to one-dimensional compression. *Géotechnique Letters*, 4(3), 223–229.
585 <https://doi.org/10.1680/geolett.14.00039>
- 586 Yan, W. M., & Su, D. (2017). Inferring 3D particle size and shape characteristics from projected 2D images:
587 Lessons learned from ellipsoids. *Computers and Geotechnics*, (September), 0–1.
588 <https://doi.org/10.1016/j.compgeo.2017.11.015>
- 589 Yu, W., & Hancock, B. C. (2008). Evaluation of dynamic image analysis for characterizing pharmaceutical
590 excipient particles. *International Journal of Pharmaceutics*, 361(1–2), 150–157.
591 <https://doi.org/10.1016/j.ijpharm.2008.05.025>
- 592 Zhou, B., & Wang, J. (2017). Generation of a realistic 3D sand assembly using X-ray micro-computed
593 tomography and spherical harmonic-based principal component analysis. *International Journal for*
594 *Numerical and Analytical Methods in Geomechanics*, 41(1), 93–109. <https://doi.org/10.1002/nag.2548>
- 595